THE JOURNAL OF PHYSICAL CHEMISTRY LETTERS
A JOURNAL OF THE AMERICAN CHEMICAL SOCIETY

pubs.acs.org/JPCL

Letter

Residue-Specific High-Resolution ^{17}O Solid-State Nuclear Magnetic Resonance of Peptides: Multidimensional Indirect ^{1}H Detection and Magic-Angle Spinning

Ivan Hung,* Eric G. Keeler, Wenping Mao, Peter L. Gor'kov, Robert G. Griffin, and Zhehong Gan

Cite This: *J. Phys. Chem. Lett.* 2022, 13, 6549–6558

Read Online

ACCESS | Metrics & More | Article Recommendations | Supporting Information

ABSTRACT: Oxygen is an integral component of proteins but remains sparsely studied because its only NMR active isotope, ^{17}O, has low sensitivity, low resolution, and large quadrupolar couplings. These issues are addressed here with efficient isotopic labeling, high magnetic fields, fast sample spinning, and ^{1}H detection in conjunction with multidimensional experiments to observe oxygen sites specific to each amino acid residue. Notably, cross-polarization at high sample spinning frequencies provides efficient $^{13}C \leftrightarrow {}^{17}O$ polarization transfer. The use of ^{17}O for initial polarization is found to provide better sensitivity per unit time compared to ^{1}H. Sharp isotropic ^{17}O peaks are obtained by using a low-power multiple-quantum sequence, which in turn allows extraction of quadrupolar parameters for each oxygen site. Finally, the potential to determine sequential assignments and long-range distance restraints is demonstrated by using 3D $^{1}H/^{13}C/^{17}O$ experiments, suggesting that such methods can become an essential tool for biomolecular structure determination.

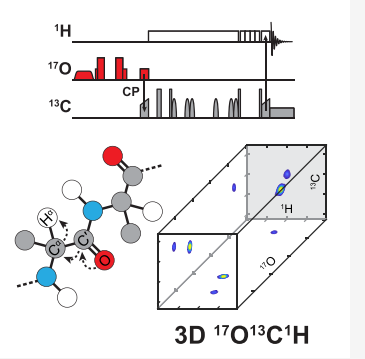

^{1}H, ^{13}C, and ^{15}N are the three key NMR-active elements that constitute the backbone and side chains of proteins. Multidimensional, multinuclear experiments using these spin $I = 1/2$ nuclei, which are "NMR-friendly" in terms of line widths and relaxation, form the basis of biomolecular NMR spectroscopy. The other key element that constitutes proteins, oxygen, has not been widely exploited despite its importance in the structure and function of biomolecules, such as in hydrogen bonding and cation interactions. The reason for this is that the single NMR-active isotope of oxygen, ^{17}O, is a spin $S = 5/2$ nucleus with low natural abundance (0.037%) and large quadrupolar interactions with the surrounding electric field gradients (EFGs). These factors make ^{17}O NMR spectra difficult to observe because of their low spectral sensitivity and resolution compared to the aforementioned $I = 1/2$ species. However, in the past few years, several approaches have been reported to address these obstacles. First, new methods to ^{17}O label peptides and carbohydrates using synthetic and acid-catalyzed exchange methods have been reported.[1−6] Notably, ^{17}O labeled amino acids have been selectively incorporated into recombinant proteins making ^{17}O NMR feasible for biomacromolecules.[7,8] Recently, mechanochemistry has also been shown to be a robust and economic method for ^{17}O enrichment of a variety of compounds.[9−12] Second, higher field NMR magnets and instrumentation have also contributed greatly to facilitating ^{17}O NMR spectroscopy. Magnetic fields up to 35.2 T have provided dramatic enhancements in spectral resolution and sensitivity through reduction of the second-order quadrupolar broadening, as illustrated in spectra of peptides and metal−organic frameworks (MOFs).[2,6,8,13,14] Third, cryogenic magic-angle spinning (MAS) probes and dynamic nuclear polarization have recently been used to yield a multifold increase in much needed spectral sensitivity.[6,15,16] Finally, solid-state NMR methods such as multiple-quantum magic-angle spinning (MQMAS)[17] and satellite-transition magic-angle spinning (STMAS)[18] which provide high-resolution isotropic spectra of half-integer quadrupolar nuclei are becoming increasingly popular for ^{17}O experiments.

Collectively, these advances have greatly facilitated ^{17}O NMR spectroscopy, allowing use of the ^{17}O chemical shift and quadrupolar parameters combined with DFT calculations to be used as sensitive probes of oxygen sites in biomolecules.[19] Indirect detection via nearby sensitive $I = 1/2$ nuclei, such as ^{1}H, can dramatically improve the sensitivity of ^{17}O NMR spectroscopy. In the past, indirect detection has been used almost exclusively in solution biomolecular NMR to detect the less sensitive ^{13}C and ^{15}N nuclei. By using heteronuclear correlation, the ^{1}H, ^{13}C, and ^{15}N resonances can be dispersed in multiple dimensions via selective one-bond coherence transfers to achieve site resolution, making assignment of sequential amino acid residues possible. The advent of MAS with spinning frequencies up to ∼100 kHz has facilitated

Received: June 9, 2022
Accepted: July 11, 2022
Published: July 13, 2022

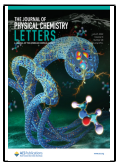

https://doi.org/10.1021/acs.jpclett.2c01777
J. Phys. Chem. Lett. 2022, 13, 6549−6558

adoption of this approach to solid-state NMR due to the improved ^{1}H line widths and sensitivity.[20−22] Also important is the fact that T_2 and $T_{1\rho}$ relaxation times are lengthened, which is crucial to the coherence transfer required for indirect detection and correlation experiments.[21]

In this paper, we report high field (18.8 T), multidimensional ^{1}H/^{13}C/^{17}O experiments using MAS at $\omega_r/2\pi$ = 90 kHz and ^{1}H detection. These experiments enable the measurement of ^{17}O chemical shift and EFG parameters of oxygen sites that are resolved by the ^{1}H and ^{13}C chemical shifts of correlated sites. In addition, MQMAS is incorporated to remove the second-order quadrupolar broadening to obtain isotropic ^{17}O resolution with line widths similar to I = 1/2 spins. ^{17}O/^{13}C correlations beyond one bond are also detected and show the potential for sequential assignment of peptide residues and identification of long distance restraints. These experiments extend recent work by others on heteronuclear correlation and distance measurement with ^{17}O on a variety of samples.[2,5,23−27] In particular, we focus on the optimal source of initial polarization, coherence transfer routes, and methods for multinuclear ^{1}H/^{13}C/^{17}O correlation with consideration for relaxation, spin-locking properties, and the spin quantum number (S = 5/2) of ^{17}O nuclei. The cross-polarization (CP) and dipolar refocused insensitive nuclei enhanced by polarization transfer (D-RINEPT) methods are compared for the key ^{17}O → ^{13}C coherence transfer to obtain optimal efficiency. The recently reported low-power MQMAS[28,29] pulse sequence is adopted to obtain ^{17}O isotropic resolution. The current study is restricted to a single [U-^{13}C, ^{15}N, 70%-^{17}O] enriched *N*-acetyl-L-valyl-L-leucine (N-Ac-VL) model peptide sample as a stepping stone to studying proteins and the three nuclei ^{1}H, ^{13}C, and ^{17}O due to the current availability of *only* a triple-resonance ultrafast MAS probe. Correlation among all four constituent nuclei in peptides (i.e., ^{1}H, ^{13}C, ^{15}N, and ^{17}O) is possible once a quadruple-resonance probe is available, thus providing additional resolution via a ^{15}N dimension and/or sharper ^{1}H line widths from the use of perdeuterated samples with back-exchanged amide protons.[30]

Many multidimensional ^{1}H/^{13}C/^{15}N experiments employing ^{13}C or ^{1}H detection have been developed for peptide and protein samples. A key element necessary to incorporate ^{17}O nuclei into such experiments is the ^{13}C ↔ ^{17}O polarization transfer which establishes ^{13}C−^{17}O correlation. Transfer of polarization to or from quadrupolar nuclei, such as ^{17}O, is an area of active research due to the complex behavior of multilevel quadrupolar spin systems under radio-frequency (rf) irradiation and MAS.[31−34] The use of cross-polarization (CP) for quadrupolar nuclei often yields mixed results, in contrast to the case of spin I = 1/2 nuclei, because the necessary spin-locking tends to be less efficient for quadrupolar nuclei. Reports of CP for quadrupolar nuclei typically employ it for selection of sites proximal to other nuclei of interest[35−37] and, more recently, also for enhancement via dynamic nuclear polarization (DNP).[38,39] For CP, continuous rf fields spin-lock the polarization of both spin species. Their rf fields match the modified Hartman−Hahn conditions during MAS and result in flip-flop and flop-flop dipolar Hamiltonians under the ZQ and DQ CP matching conditions, respectively.[40] The dipolar Hamiltonian mediates spin exchange between the two species. It is noteworthy that in the case of a ^{13}C site coupled to two ^{17}O sites the flip-flop terms for the two C−O dipolar Hamiltonians do not commute. The weaker dipolar Hamiltonian is effectively truncated by the strong one, limiting CP to the weakly coupled spin, resulting in so-called "dipolar truncation".[41,42] Thus, CP is preferable for directly bonded ^{13}C−^{17}O sites but is suboptimal for probing long-range correlations in the presence of short contacts. The application of CP for ^{17}O is investigated here since its use at high MAS frequencies is relatively unexplored in the literature. An alternative method for polarization transfer which has been shown to be robust at slow to moderate spinning frequencies is D-RINEPT technique.[43] INEPT transfers do not experience dipolar truncation, as the relevant dipolar Hamiltonians commute, making the transfer suitable in principle for long-range correlation and distance measurements. However, long-range transfers naturally deduct efficiency from short-range transfers. Notably, dipolar heteronuclear multiple-quantum correlation (D-HMQC) methods[44,45] are not considered here because they depend on the subtraction of unwanted signals, which results in a tendency to exhibit severe t_1 noise for sites with large chemical shift anisotropy under even minor MAS instability, which can often be worse at higher spinning frequencies, though methods to alleviate the t_1-noise have been reported.[46] Furthermore, an efficient D-HMQC method for obtaining isotropic spectra of the indirectly detected quadrupolar nucleus has so far been elusive.

Figure 1 compares the carbonyl region of the ^{13}C NMR spectra of N-Ac-VL acquired by using ^{17}O → ^{13}C CP and D-RINEPT. The CP spectrum shows ca. 40 and 78% higher signal-to-noise ratios (s/n) for the Leu and Val C′ peaks,

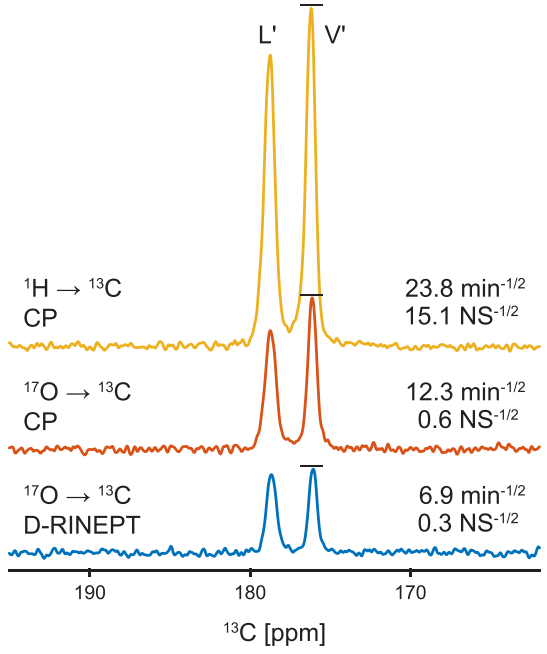

Figure 1. Carbonyl region of the ^{13}C NMR spectra of N-Ac-VL acquired using (top) ^{1}H → ^{13}C CP, (middle) ^{17}O → ^{13}C CP, and (bottom) ^{17}O → ^{13}C D-RINEPT with the ^{13}C carrier frequency placed on the V′ peak. All spectra are normalized by their root-mean-square noise. The numerical values shown on the spectra are the signal-to-noise ratios for the V′ peak as a function of the square root of the experimental time $S(t)$ or the number of scans $S(n)$. The ^{17}O → ^{13}C CP and D-RINEPT spectra were enhanced by a factor of ∼3 for N-Ac-VL by satellite-transition saturation/inversion using an off-resonance WURST pulse. Total experimental times for the three spectra were (top) 52 min, (middle) 38 min, and (bottom) 37 min.

https://doi.org/10.1021/acs.jpclett.2c01777
J. Phys. Chem. Lett. 2022, 13, 6549−6558

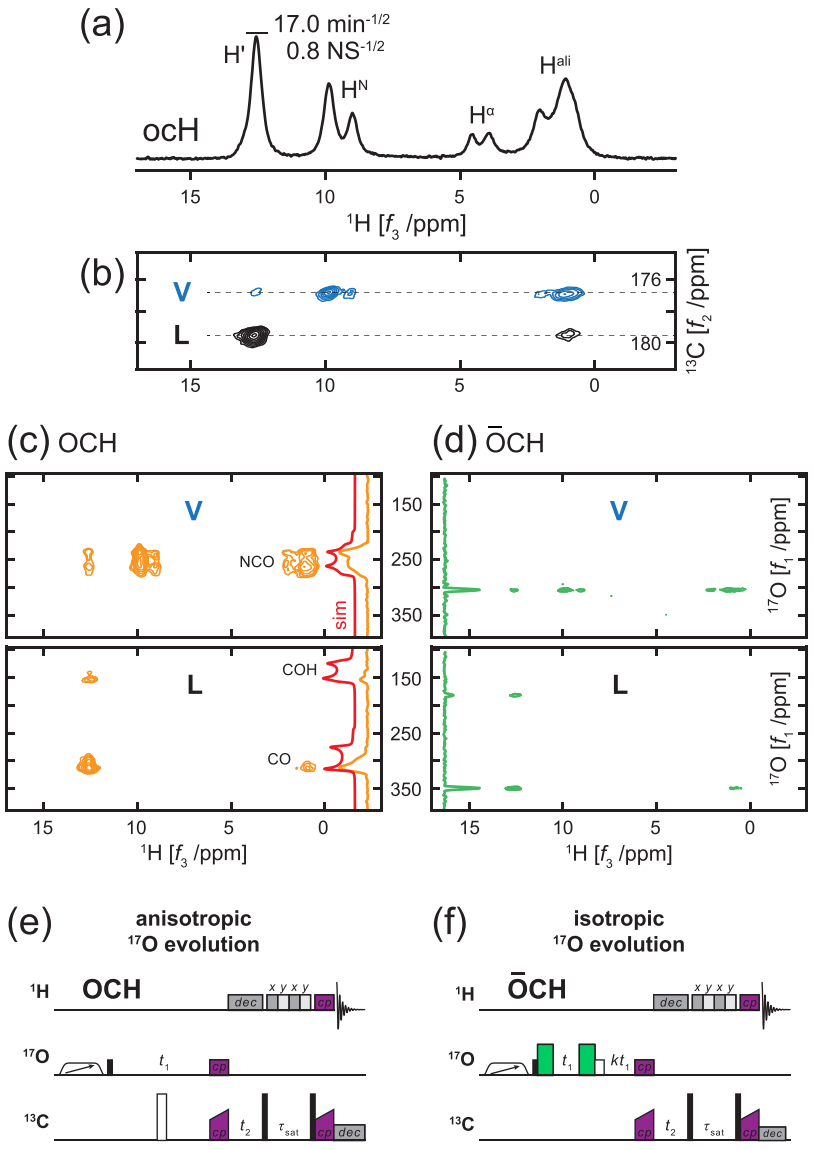

Figure 2. (a) ^{1}H-detected 1D ocH NMR spectrum of N-Ac-VL. The numerical values correspond to $S(t)$ and $S(n)$ for the hydroxyl ^{1}H peak. (b) 2D CH projection of the 3D OCH spectrum of N-Ac-VL. (c, d) 2D OH planes from the OCH spectrum at the ^{13}C shifts (dashed lines) for the C′ sites of Val and Leu with (c) anisotropic and (d) isotropic ^{17}O detection, which were acquired with the pulse sequences depicted in (e) and (f), respectively. Simulated ^{17}O quadrupolar patterns in (c) are shown as red traces. Isotropic ^{17}O evolution in (d) is achieved by using cos-lpMQMAS and split-t_1 acquisition with a factor $k = 19/12$ for spin $S = 5/2$ nuclei as shown in (f). CP contact times of 4.0 and 0.8 ms were used for the ^{17}O → ^{13}C and ^{13}C → ^{1}H transfers, respectively. Total experimental times for the spectra were (a) 3.4 h for 1D ocH, (b, c) ∼7 h for 3D OCH, and (b, d) ∼7 h for 3D ŌCH.

respectively, compared to D-RINEPT. Notably, when optimized for the C′ sites, none of the other ^{13}C sites are polarized by using either method. For fast MAS frequencies, the $n = 1$ double-quantum (DQ) CP condition[40,47−49] is typically used for its low rf power requirements, where the sum of the rf amplitudes ω_1 for the two nuclei is equal to the spinning frequency ω_r. The effective nutation frequency of the ^{17}O central transition is scaled by the factor $(S + 1/2)$ when ω_1 is small compared to the quadrupole coupling interaction,[31,50] which constitutes the majority of cases. Therefore, the DQ Hartman−Hahn matching condition needs to be modified to $\omega_{1C} + 3\omega_{1O} = \omega_r$. The rf amplitudes employed in Figure 1 were $\omega_{1C} \approx 0.75\omega_r$ and $3\omega_{1O} \approx 0.25\omega_r$ with $\omega_r/2\pi = 90$ kHz. These rf fields were optimized to consider the spin-lock relaxation time $T_{1\rho}$ and chemical shift offsets. In particular, the rf field strengths need to avoid the primary rotary resonance condition $\omega_{1C} = 3\omega_{1O} = \omega_r$ to the extent possible, while reducing leakage of ^{17}O polarization from the central transition to other transitions, which increases proportionally with the ^{17}O rf field amplitude. In addition to improved sensitivity, the low rf fields used for CP cause less rf sample heating and are less taxing on probe hardware than for D-RINEPT, which requires a ^{13}C rf field of $\omega_{1C} = 2\omega_r$; 180 kHz in the current case.

The seminal papers by Vega[31,32] have shown that there are two regimes where spin locking is relatively effective for quadrupolar nuclei. Namely, when the adiabaticity parameter α meets the conditions $\alpha \gg 1$ or $\alpha \ll 1$, where $\alpha = (S + 1/2)^2\omega_1^2/(\omega_Q\omega_r)$, ω_1 is the amplitude of the applied rf field, ω_r is the sample spinning frequency, and $\omega_Q/2\pi = 3C_Q/[2S(2S - 1)]$ is the quadrupole coupling frequency defined by the quadrupole coupling constant C_Q and the spin quantum number S. The available hardware often

https://doi.org/10.1021/acs.jpclett.2c01777
J. Phys. Chem. Lett. 2022, 13, 6549−6558

limits the combinations of ω_1 and ω_r that can be chosen to avoid being close to the $\alpha \sim 1$ condition where spin locking and CP perform poorly. The $\alpha \gg 1$ condition requires relatively high rf fields, which can give rise to excessive sample heating and hardware damage during long spin-lock times, generally disfavoring its use. Thus, the $\alpha \ll 1$ condition tends to be the more practical choice. The ZQ and DQ CP matching conditions[40] constrain the rf fields for the spin $I = 1/2$ and $S > 1/2$ nuclei to be within $2\omega_r$ from each other. Therefore, if ω_1 must remain low for the $S > 1/2$ nuclei to satisfy the $\alpha \ll 1$ spin-locking condition, for example, $(S + 1/2)\omega_{1S} < \omega_r$, then the rf field for the $I = 1/2$ nuclei must remain less than $3\omega_r$ to achieve CP. However, using rf amplitudes lower than $3\omega_r$ usually leads to poor spin-locking at low spinning frequencies due to interference from the broad rotary resonance recoupling (R^3) conditions found at $\omega_1 = \omega_r/2$, ω_r, and $2\omega_r$.[51,52] This problem is particularly acute for ^{1}H nuclei with strong homonuclear dipolar coupling. The breadths of the R^3 conditions become sharper at high MAS frequencies due to improved averaging of the CSA and dipolar coupling interactions, allowing the use of ω_1 values interleaved between the R^3 conditions. Hence, the DQ CP conditions ($\omega_{1C} + 3\omega_{1O} = n\omega_r$; $n = 1, 2$) become increasingly viable with faster spinning rates.[47,49] If a threshold of $\alpha < 0.05$ is assumed to provide effective spin-locking, then under the experimental conditions used here ($\omega_r/2\pi$ = 90 kHz, $3\omega_{1O} \sim 0.25\omega_r$) efficient CP would be expected for any ^{17}O nuclei with C_Q values greater than 750 kHz, that is, the full range of C_Q relevant to biological and organic samples (6−11 MHz).[19] In this regard, the use of fast MAS appears to provide significant potential for application of CP to quadrupolar systems which were less amenable in the past due to slower spinning.

There are usually large differences in T_1 relaxation between ^{17}O and ^{1}H. The quadrupolar interaction typically dominates ^{17}O T_1 relaxation and results in much shorter T_1 values than for ^{1}H. Furthermore, ^{1}H T_1 values often increase at high MAS frequencies due to reduced spin-diffusion to mobile and fast relaxing ^{1}H sites, though this can be remedied by reintroduction of spin diffusion.[53] The ^{1}H T_1 relaxation time observed for the N-Ac-VL sample (~4.5 s) at $\omega_r/2\pi$ = 90 kHz is more than 2 orders of magnitude longer than for ^{17}O (~15 ms). The s/n per square root of time $S(t)$ for the C′ carbons in Figure 1 is surprisingly high, at ~52% for ^{17}O → ^{13}C CP compared to ^{1}H → ^{13}C CP, which serves as a point of reference for the sensitivity. Included in this value of $S(t)$ is an ~3-fold enhancement of the ^{17}O central-transition polarization by application of a WURST pulse prior to ^{17}O excitation. This enhancement, together with the short ^{17}O T_1 relaxation, significantly boosts $S(t)$; more than what would be expected from a comparison of the ^{1}H and ^{17}O receptivities. If the s/n per square root of the number of scans $S(n)$ is compared instead, then the higher ^{1}H receptivity provides a clear advantage for ^{1}H → ^{13}C CP, being ~25-fold better than ^{17}O → ^{13}C CP.

Having established a viable method for ^{17}O → ^{13}C polarization transfer, it should then be straightforward to incorporate it into commonly used ^{1}H-detected heteronuclear experiments. The simplest is the concatenation of two CP steps, ^{17}O → ^{13}C CP followed by ^{13}C → ^{1}H CP, in analogy to hnH and hcH experiments,[54,55] but with ^{17}O as the starting source of polarization instead of ^{1}H. A 1D ocH spectrum for N-Ac-VL acquired by using the pulse sequence in Figure 2e is shown in Figure 2a. (The naming convention used in this work to describe pulse experiments is as follows: lower case letters denote nuclei that take part in the polarization transfer pathway used in the pulse sequence but are not observed, while upper case letters denote nuclei that are observed, or evolved, during multidimensional experiments.) The first ^{17}O → ^{13}C CP transfer is selective as observed in Figure 1; however, the subsequent ^{13}C → ^{1}H CP step from the C′ carbons to protons is not. The resonances for all ^{1}H sites in the sample are observed because a relatively long ^{13}C → ^{1}H contact time is required due to the absence of directly bonded H atoms on the C′ nuclei. Notably, the $S(t)$ for the ocH experiment with two coherence transfers, ^{17}O → ^{13}C followed by ^{13}C → ^{1}H, is improved by ~40% compared to the ^{17}O → ^{13}C CP spectrum in Figure 1, reiterating the sensitivity advantage of ^{1}H indirect detection. Acquisition of a full 3D OCH experiment allows separation of the ^{17}O quadrupolar patterns associated with each C′ site. The 2D CH projection of the OCH spectrum for N-Ac-VL is shown in Figure 2b, and the OH planes associated with the ^{13}C′ resonances of the Val and Leu residues are shown in Figure 2c. The three different ^{17}O sites in N-Ac-VL, denoted NCO for the amide moiety on Val and COH and CO for the protonated and unprotonated oxygen sites on the carboxylate group of Leu, are clearly resolved and can be assigned unambiguously to their respective residues. However, the observed ^{17}O patterns (orange traces) show intensity distortions compared to the ideal patterns (red traces), as has been reported previously,[56−59] which can lead to errors in ^{17}O quadrupolar parameters determined by using the line shapes. More accurate line shapes can be obtained by using D-RINEPT;[43] however, the significant sensitivity advantage provided by CP is favored here since sensitivity is expected to be a major obstacle for investigation of large biomolecules.

It is possible to substitute the conventional anisotropic ^{17}O t_1 evolution period in Figure 2e with isotropic ^{17}O detection by incorporation of a split-t_1 cos-lpMQMAS sequence[28,29] as shown in Figure 2f. The resulting 3D $\bar{\text{O}}$CH experiment yields the same 2D CH projection as in Figure 2b, but now the ^{17}O signals in the 2D OH planes become sharp resonances as shown in Figure 2d (an overbar is used here to denote experiments with "averaged" or isotropic ^{17}O evolution). Importantly, the isotropic ^{17}O line widths are obtained by refocusing the second-order quadrupolar coupling and are therefore largely independent of the external magnetic field. The greatly reduced line width along with the large chemical shift range of ^{17}O alludes to its immense potential as a source of signal dispersion, in complement to ^{1}H, ^{13}C, and ^{15}N nuclei, for the resolution of congested spectra. The combination of isotropic and anisotropic ^{17}O detection can also be used to extract the composite quadrupolar product P_Q for each oxygen site by simply comparing the center of mass δ_c of the ^{17}O resonances between the two spectra, as detailed below. Both the ^{17}O chemical shift and EFG parameters are sensitive probes of the oxygen structure, bonding, and electronic environments.[19]

For peptide samples, the 3D OCH experiments presented above do not provide sufficient site specificity because the polarization that resides on C′ after ^{17}O → ^{13}C CP is distributed to all proximate ^{1}H sites. It would be more desirable to first transfer polarization from the C′ to the C$^\alpha$ sites before a short ^{13}C → ^{1}H CP step is used for H$^\alpha$ detection, so that each ^{17}O, ^{13}C, and ^{1}H site gives rise to a single resonance in 3D spectra. This can be achieved by using the

https://doi.org/10.1021/acs.jpclett.2c01777
J. Phys. Chem. Lett. 2022, 13, 6549−6558

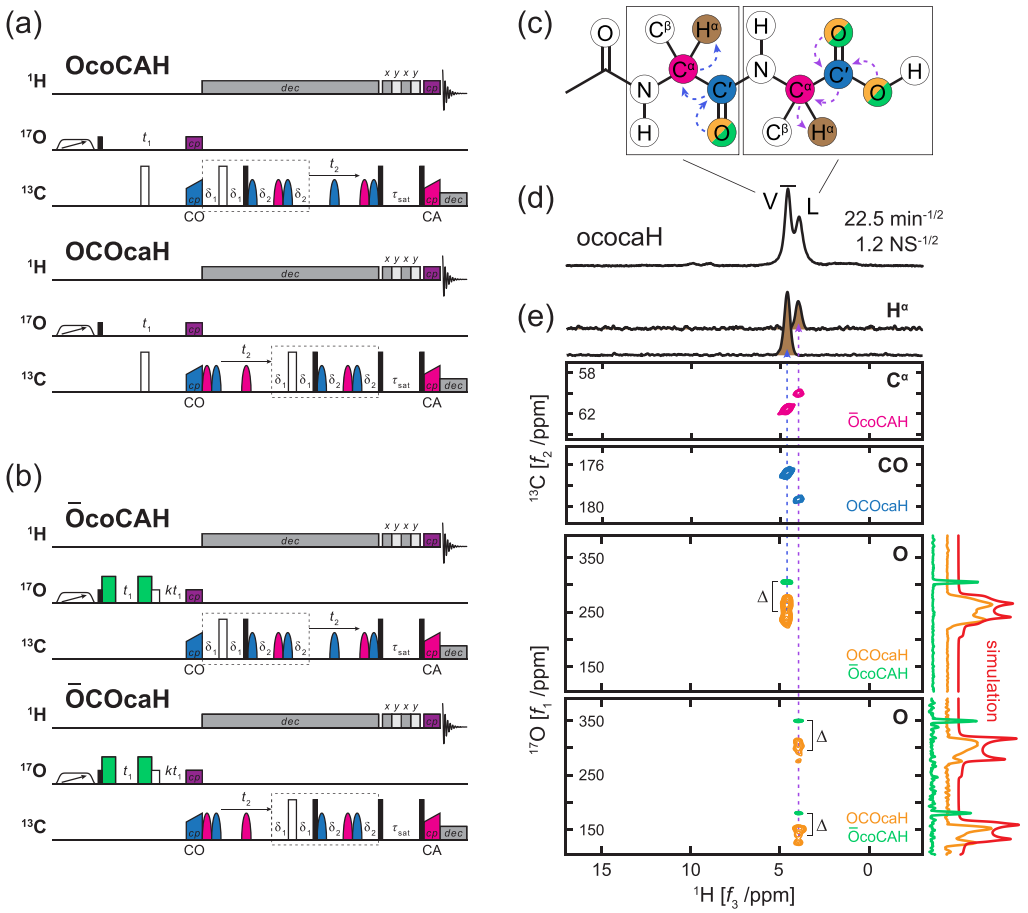

Figure 3. Pulse sequence diagrams for ^{1}H-detected 3D OCH experiments with incorporation of homonuclear C′ → C$^{\alpha}$ transfer (dashed rectangle) and either (a) anisotropic or (b) isotropic ^{17}O detection. Blue and magenta pulses on the ^{13}C channel are applied with the transmitter offset centered on the C′ and C$^{\alpha}$ sites, respectively. (c) Schematic depicting the polarization transfer pathways used in the OCH experiments, starting from the ^{17}O sites and ending on the H$^{\alpha}$ nuclei. (d) ^{1}H-detected 1D ococaH NMR spectrum of N-Ac-VL. The numerical values correspond to $S(t)$ and $S(n)$ for the Val C$^{\alpha}$ ^{1}H peak. (e) 2D planes from 3D ŌcoCAH and OCOcaH spectra showing clear resolution of each O, C′, C$^{\alpha}$, and H$^{\alpha}$ site corresponding to the Val and Leu residues in N-Ac-VL. The difference Δ in the center of mass for the anisotropic and isotropic ^{17}O resonances provides a simple method to determine the quadrupole coupling of each oxygen site (see eq 1). Simulated ^{17}O quadrupolar patterns are shown as red traces. Total experimental times for the spectra were (d) 3.4 h for 1D ococaH and (e) ∼8 h each for 3D OCOcaH and 3D ŌcoCAH.

scalar J-coupling-based homonuclear ^{13}C−^{13}C INEPT technique, as has been shown in the literature.[20−22,60] The resulting pulse sequences with anisotropic and isotropic ^{17}O evolution are shown in Figures 3a and 3b, respectively. A 1D ococaH spectrum of N-Ac-VL is shown in Figure 3d, displaying a remarkably high $S(t)$ of 22.5 min$^{-1/2}$ for the Val H$^{\alpha}$ resonance. For reference, an analogous experiment employing ^{15}N instead of ^{17}O, namely hncocaH, has been reported to have an average $S(t)$ of ∼3 min$^{-1/2}$ for the 56 amino acid residues in a GB1 protein sample.[22] It is noteworthy that an increase in sensitivity for the ococaH spectrum (Figure 3d) is observed compared to the ocH spectrum in Figure 2a, even with the additional C′−C$^{\alpha}$ polarization transfer step due to the concentration of all the signal into the H$^{\alpha}$ sites.

With selective one-bond polarization transfer, the suite of 3D experiments in Figure 3 give rise to one peak for each ^{1}H, ^{13}C, and ^{17}O site, except for the C-terminus residue, which allows straightforward peak assignments. For the N-Ac-VL dipeptide, the C-terminus leucine is easily identified by the presence of its two COOH oxygen signals as shown in Figure 3e. Then, the C′, C$^{\alpha}$, and H$^{\alpha}$ resonances of the two residues can be simply identified and traced back from the 2D projections. The 2D OH planes in Figure 3e are overlays of spectra acquired with anisotropic ^{17}O MAS evolution and isotropic ^{17}O evolution obtained by incorporation of split-t_1 cos-lpMQMAS. The difference in the center of mass for the ^{17}O resonances in the two 3D spectra can yield the magnitude of the quadrupole coupling P_Q for each site without the need for spectral simulation or line shape fitting, circumventing the need for accurate quadrupolar line shapes, albeit with slightly less accuracy. In anisotropic ^{17}O spectra, resonances are centered at the sum of the isotropic chemical shift δ_{iso} and quadrupole induced shift δ_{QIS}, that is, $\delta_c(^{17}O) = \delta_{iso} + \delta_{QIS}$, whereas the corresponding peaks in isotropic ^{17}O spectra appear at $\delta_c(^{17}\bar{O}) = \delta_{iso} - (10/17)\delta_{QIS}$. Therefore, their difference in units of ppm is equal to $\Delta = \delta_c(^{17}O) - \delta_c(^{17}\bar{O}) = (27/17)\delta_{QIS}$, where $\delta_{QIS} = -6000(P_Q^2/\nu_0^2)$ for $S = 5/2$ nuclei such as ^{17}O, and thus the quadrupolar product is given by

$$P_Q = \sqrt{-\frac{17}{27}\frac{\Delta\nu_0^2}{6000}} \quad (1)$$

in units of hertz, where ν_0 is the Larmor frequency. The Δ values measured for the NCO, CO, and COH sites of N-Ac-VL are −58, −59, and −45 ppm which give ^{17}O $P_Q = C_Q(1 + \eta_Q^2/3)^{1/2}$ of 8.5, 8.5, and 7.5 MHz,

https://doi.org/10.1021/acs.jpclett.2c01777
J. Phys. Chem. Lett. 2022, 13, 6549−6558

respectively, in good agreement with values previously obtained from line shape fitting.[2]

Aside from providing residue-specific ^{17}O information including both the chemical shift and quadrupolar coupling parameters, the exceptional resolution and shift dispersion afforded by isotropic ^{17}O detection also offers the potential for sequential assignment of polypeptide backbone ^{13}C sites in a way similar to that performed with ^{1}H/^{13}C/^{15}N experiments. We are not able as of yet to perform relayed one-bond polarization transfers between adjacent i and $(i + 1)$ residues as the inclusion of ^{15}N requires a quadruple-resonance ^{1}H/^{13}C/^{15}N/^{17}O probe. An alternative option would be to perform direct polarization transfer from ^{17}O to ^{13}C$^{\alpha}$ nuclei. However, this is relatively inefficient and requires long contact times due to weak dipolar coupling. The result of such a ^{17}O → ^{13}C$^{\alpha}$ CP spectrum for N-Ac-VL (not shown) gives only ∼20% the s/n compared to the ^{17}O → ^{13}C′ CP spectrum in Figure 1. A more efficient approach takes advantage of the stronger dipolar coupling between C′ and C$^{\alpha}$ nuclei, and their longer T_2 and $T_{1\rho}$, to create inter-residue correlations. To this end, the J-based INEPT C′ → C$^{\alpha}$ transfer in the OcoCAH and ŌcoCAH experiments (Figure 3) can be replaced with the dipolar recoupling enhancement through amplitude modulation (DREAM) scheme,[61] as shown in Figure 4b. The INEPT and DREAM methods have been shown to provide similar one-bond C′ → C$^{\alpha}$ transfer efficiency (∼40%) for ^{1}H-detected experiments under fast MAS conditions.[21] However, the DREAM sequence is more appropriate in this instance because the J-coupling necessary for INEPT between the i C′ and $(i + 1)$ C$^{\alpha}$ sites is vanishingly small. The experiment incorporating DREAM, dubbed Ō<u>coCA</u>H (the underline is used to denote long-range correlation), is shown in Figure 4b along with a schematic of the polarization transfer pathway. In complement to OcoCAH (Figure 4a), where each ^{17}O site correlates to a single peak (Figure 4c, blue), the 3D Ō<u>coCA</u>H experiment (Figure 4b) gives rise to two sets of C$^{\alpha}$/H$^{\alpha}$ peaks for each ^{17}O site: one from the i residue and one from the adjacent $(i + 1)$ residue (Figure 4c, red), in analogy to HNCA experiments used in solution NMR spectroscopy.[62,63] Thus, sequential assignment of backbone ^{13}C sites can be made in conjunction with the other 3D experiments presented above.

Surprisingly, the Leu ^{17}O sites show a weak correlation with the Val C$^{\alpha}$/H$^{\alpha}$ peaks which is not expected a priori. Long-range polarization transfer in the Ō<u>coCA</u>H experiment (Figure 4b) occurs during the DREAM step, and negligible transfer would be expected between the Leu C′ and Val C$^{\alpha}$ sites due to the relative long distance between them. Inspection of the N-Ac-VL crystal structure shows that the two nearest Leu C′ to Val C$^{\alpha}$ distances are to the inter-residue site and an intermolecular site, both of which are ∼4.45 Å in length. This observation raises the prospect of applying the Ō<u>coCA</u>H sequence not only for backbone assignment through inter-residue correlations but also for identification of longer distance secondary structure restraints or interpeptide correlations.

All 3D experiments presented above begin with ^{17}O instead of ^{1}H polarization due to improved sensitivity resulting from the much faster ^{17}O T_1 relaxation observed at room temperature for the N-Ac-VL sample. These experiments can be modified by substituting the initial ^{17}O excitation portion of the pulse sequences with a ^{1}H → ^{17}O CP transfer step. A comparison of 1D spectra obtained in this way with the previously shown spectra, which employed ^{17}O polarization, is

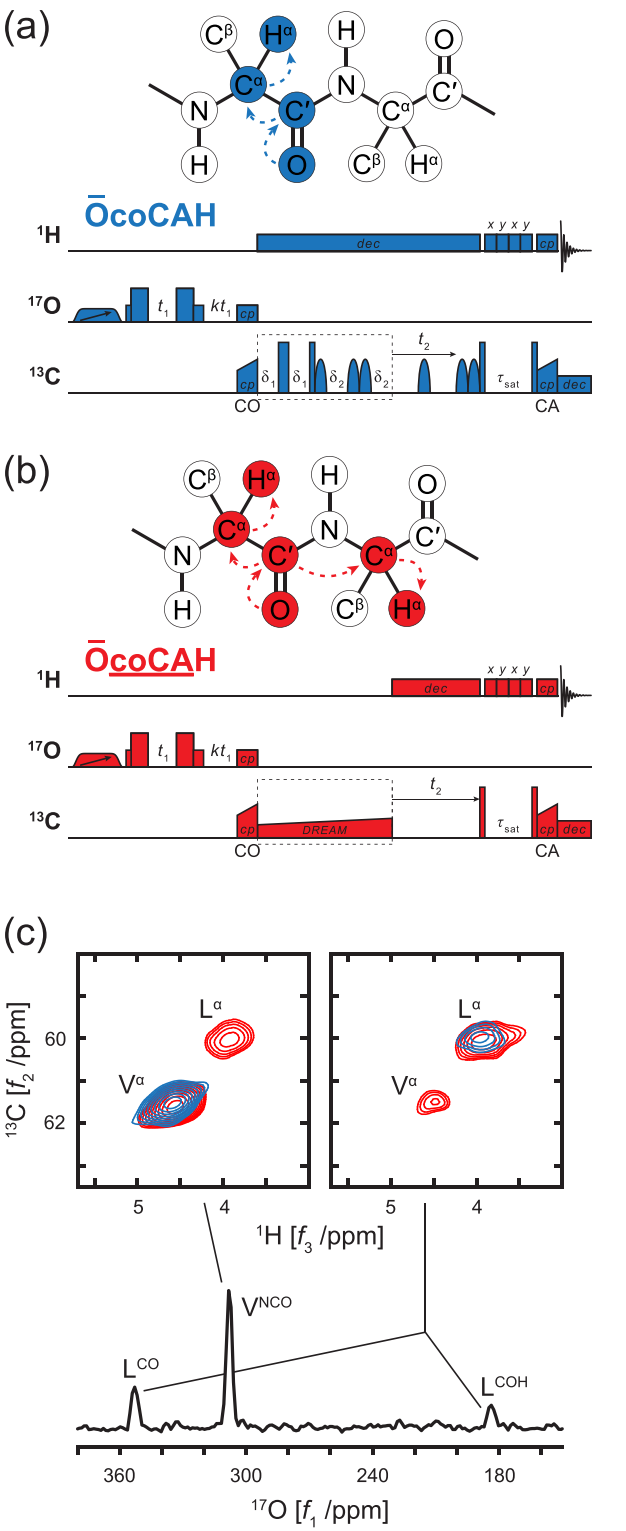

Figure 4. Pulse sequence diagrams and polarization transfer pathways for the 3D ^{1}H-detected (a) ŌcoCAH and (b) Ō<u>coCA</u>H experiments which correlate ^{17}O sites with the C$^{\alpha}$/H$^{\alpha}$ sites of only the i residue or with both the i and $(i + 1)$ residues, respectively. (c) Overlay of 2D CAH planes from the ŌcoCAH (blue) and Ō<u>coCA</u>H (red) experiments performed on N-Ac-VL showing the presence of inter-residue O/C$^{\alpha}$ correlations for the latter experiment as opposed to only intraresidue correlations in the former. A DREAM mixing time of 12 ms was used for the long-range C′ to C$^{\alpha}$ polarization transfer. Total experimental times for the spectra in (e) were ∼8 h for 3D ŌcoCAH and ∼22 h for 3D Ō<u>coCA</u>H.

https://doi.org/10.1021/acs.jpclett.2c01777
J. Phys. Chem. Lett. 2022, 13, 6549−6558

shown in Figure 5. The $S(t)$ is once again significantly better by using ^{17}O polarization. However, examination of $S(n)$ site, which is a sensitive probe of the ^{17}O environment, can be obtained by comparison of spectra with isotropic and anisotropic ^{17}O evolution. It can be envisioned that 2D ŌcocaH spectra could serve as "fingerprints" for the investigation of protein structural changes due to activity, folding, drug binding, and other native or induced perturbations.

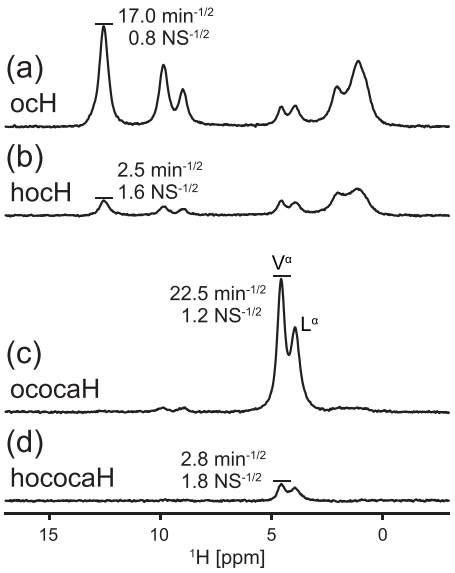

Figure 5. Heteronuclear ^{1}H-detected NMR spectra of N-Ac-VL acquired with initial polarization from (a, c) ^{17}O, or (b, d) ^{1}H nuclei and (a, b) without or (c, d) with homonuclear $C' \rightarrow C^{\alpha}$ INEPT transfer. The numerical values correspond to $S(t)$ and $S(n)$ for the hydroxyl ^{1}H peak in (a, b) and the Val C^{α} ^{1}H peak in (c, d). The total experimental time for the each 1D spectrum was ∼3.4 h.

shows that experiments employing initial ^{1}H polarization have an advantage of ∼1.5 to 2.0 instead. Thus, under conditions where the ^{1}H and ^{17}O T_1 relaxation times are more comparable, or the ^{1}H polarization is significantly enhanced by application of DNP,[64−66] the sensitivity of the presented experiments may be tipped in favor of using ^{1}H polarization instead.

The experiments described here aim to demonstrate the viability of incorporating ^{17}O into the arsenal of nuclei (^{1}H, ^{13}C, and ^{15}N) commonly used for the study of structure and dynamics in peptides and proteins via solid-state NMR spectroscopy. In particular, aside from improving ^{1}H resolution and coherence lifetimes ($T_{1\rho}$ and T_2), high sample spinning frequency plays a critical role in supporting the application of low-power rf CP conditions, which in turn provides effective polarization transfer to and from ^{17}O nuclei. The applicability of CP to ^{17}O allows straightforward substitution of ^{15}N with ^{17}O in heteronuclear NCH pulse sequences reported in the literature[22] to generate analogous OCH experiments. As such, three-dimensional experiments are developed and presented here to measure residue-specific ^{17}O NMR powder patterns. Notably, experiments utilizing initial ^{17}O polarization, as opposed to ^{1}H polarization, are found to provide better sensitivity as a function of time due to the much faster ^{17}O T_1 relaxation.

In addition to the site resolution provided by correlation to the ^{1}H and ^{13}C nuclei, the ^{17}O signal resolution can be enhanced further by application of well-known multiple-quantum correlation methods. Here, the recently reported cos-lpMQMAS method is applied to obtain isotropic ^{17}O peaks, yielding spectra that are comparable to those obtained for $I = 1/2$ nuclei while also benefiting from the large ^{17}O shift range. Additionally, the quadrupole coupling for each oxygen

Experimental Methods. The *N*-acetyl-[U-^{13}C,^{15}N,70% ^{17}O]-L-valyl-L-leucine (N-Ac-VL) sample used here was prepared by ^{17}O labeling U-^{13}C,^{15}N-FMOC-L-valine and U-^{13}C,^{15}N-FMOC-L-leucine with $H_2{}^{17}O$ via a multiple turnover reaction.[1] The procedure involves reacting an FMOC, BOC, Trt, or OtBu amino acid with excess carbodiimide and in this case 70% $H_2{}^{17}O$. The reaction is a kinetically enhanced multiple turnover process that provides the ^{17}O-labeled FMOC amino acids in high yield and an isotopic enrichment equal to that of the starting $H_2{}^{17}O$. It appears to be a generally applicable approach for ^{17}O carboxyl groups. Further details of the procedure are available in refs 1 and 2.

NMR experiments were acquired at 18.8 T on a Bruker Avance III HD console using a triple-resonance probe designed and constructed at the NHMFL with a JEOL 0.75 mm MAS stator. The carrier frequencies for ^{1}H, ^{13}C, and ^{17}O were 800.12, 201.17, and 108.47 MHz, respectively. All experiments were performed at a spinning frequency $\omega_r/2\pi$ = 90 kHz. For heteronuclear dipolar recoupling in the $^{17}O-^{13}C$ D-RINEPT experiment, the $SR4^2_1$ sequence[67] was used on the ^{13}C channel at an rf field amplitude $\omega_1/2\pi$ twice the spinning frequency, 180 kHz. For experiments starting with ^{17}O polarization, the signal was enhanced by saturation/inversion of the ^{17}O satellite transitions using a WURST pulse[68,69] with a sweep width equal to the MAS frequency of 90 kHz, 1 ms pulse duration, peak rf field $\omega_1/2\pi$ = 12.4 kHz, and an offset of +450 kHz, leading to ^{17}O signal enhancement for the N-Ac-VL sample by a factor of ∼3. Other experimental parameters are given in the Supporting Information. The cosine low-power MQMAS sequence (cos-lpMQMAS)[28,29] with triple-/single-quantum split-t_1 evolution was used to obtain isotropic ^{17}O resolution by using cosine pulses with a duration of two rotor periods and a ratio $k = 19/12$ for $S = 5/2$ nuclei.[70,71]

^{1}H chemical shifts were referenced indirectly to neat tetramethylsilane (δ_{iso} = 0 ppm) by setting the highest frequency peak of histidine·HCl·H_2O to 17.2 ppm.[72] ^{13}C and ^{17}O shifts were referenced to DSS and D_2O at 0 ppm, respectively, by using the reference frequency for ^{1}H at 0 ppm and the IUPAC recommended standard frequency ratios.[73] All spectra were processed by using Bruker Topspin 4.1.1 and imported into MATLAB R2020b Update 6 (9.9.0.1718557) for analysis and plotting. For the isotropic ^{17}O dimension of 3D spectra, the axis was scaled and referenced according to the "unified" convention for MQMAS and STMAS.[74] Essentially, the ^{17}O spectral window was divided by a factor $(3 - k) = 17/12$, while keeping the Larmor frequency and shift reference the same as for conventional 1D ^{17}O spectra.

■ ASSOCIATED CONTENT

Supporting Information

The Supporting Information is available free of charge at https://pubs.acs.org/doi/10.1021/acs.jpclett.2c01777.

Additional experimental details including all parameters used in the pulse sequences and pulse sequences for the

https://doi.org/10.1021/acs.jpclett.2c01777
J. Phys. Chem. Lett. 2022, 13, 6549−6558

3D OCOcaH, ŌcoCAH, and Ō<u>coCA</u>H experiments in Bruker format (PDF)

AUTHOR INFORMATION

Corresponding Author

Ivan Hung − *National High Magnetic Field Laboratory, Tallahassee, Florida 32310, United States;* orcid.org/0000-0001-8916-739X; Email: hung@magnet.fsu.edu

Authors

Eric G. Keeler − *Department of Chemistry and Francis Bitter Magnet Laboratory, Massachusetts Institute of Technology, Cambridge, Massachusetts 02139, United States*

Wenping Mao − *National High Magnetic Field Laboratory, Tallahassee, Florida 32310, United States*

Peter L. Gor'kov − *National High Magnetic Field Laboratory, Tallahassee, Florida 32310, United States*

Robert G. Griffin − *Department of Chemistry and Francis Bitter Magnet Laboratory, Massachusetts Institute of Technology, Cambridge, Massachusetts 02139, United States;* orcid.org/0000-0003-1589-832X

Zhehong Gan − *National High Magnetic Field Laboratory, Tallahassee, Florida 32310, United States;* orcid.org/0000-0002-9855-5113

Complete contact information is available at: https://pubs.acs.org/10.1021/acs.jpclett.2c01777

Notes

The authors declare no competing financial interest.

ACKNOWLEDGMENTS

This work was supported by the National High Magnetic Field Laboratory (NHMFL, USA) through NSF DMR-1644779 and the State of Florida. In addition, we acknowledge the support of the National Institutes of Health through Grants AG058504, GM132997, and GM132079 to R.G.G. Use of the NHMFL NMR facility is available free of charge; for more information please visit https://nationalmaglab.org/user-facilities/nmr-mri.

REFERENCES

(1) Seyfried, M. S.; Lauber, B. S.; Luedtke, N. W. Multiple-Turnover Isotopic Labeling of Fmoc- and Boc-Protected Amino Acids with Oxygen Isotopes. *Org. Lett.* **2010**, *12* (1), 104−106.

(2) Keeler, E. G.; Michaelis, V. K.; Colvin, M. T.; Hung, I.; Gor'kov, P. L.; Cross, T. A.; Gan, Z.; Griffin, R. G. 17O MAS NMR Correlation Spectroscopy at High Magnetic Fields. *J. Am. Chem. Soc.* **2017**, *139* (49), 17953−17963.

(3) Yamada, K.; Yamaguchi, Y.; Uekusa, Y.; Aoki, K.; Shimada, I.; Yamaguchi, T.; Kato, K. Solid-State 17O NMR Analysis of Synthetically 17O-Enriched d-Glucosamine. *Chem. Phys. Lett.* **2020**, *749*, 137455.

(4) Dai, Y.; Wu, G. Solid-State 17O NMR Studies of Sulfonate Jump Dynamics in Crystalline Sulfonic Acids: Insights into the Hydrogen Bonding Effect. *J. Phys. Chem. A* **2020**, *124* (46), 9597−9604.

(5) Ha, M.; Nader, S.; Pawsey, S.; Struppe, J.; Monette, M.; Mansy, S. S.; Boekhoven, J.; Michaelis, V. K. Racing toward Fast and Effective 17O Isotopic Labeling and Nuclear Magnetic Resonance Spectroscopy of N-Formyl-MLF-OH and Associated Building Blocks. *J. Phys. Chem. B* **2021**, *125* (43), 11916−11926.

(6) Shen, J.; Terskikh, V.; Struppe, J.; Hassan, A.; Monette, M.; Hung, I.; Gan, Z.; Brinkmann, A.; Wu, G. Solid-State 17O NMR Study of α-d-Glucose: Exploring New Frontiers in Isotopic Labeling, Sensitivity Enhancement, and NMR Crystallography. *Chem. Sci.* **2022**, *13* (9), 2591−2603.

(7) Paulino, J.; Yi, M.; Hung, I.; Gan, Z.; Wang, X.; Chekmenev, E. Y.; Zhou, H.-X.; Cross, T. A. Functional Stability of Water Wire-Carbonyl Interactions in an Ion Channel. *Proc. Natl. Acad. Sci. U. S. A.* **2020**, *117* (22), 11908−11915.

(8) Lin, B.; Hung, I.; Gan, Z.; Chien, P.; Spencer, H. L.; Smith, S. P.; Wu, G. 17O NMR Studies of Yeast Ubiquitin in Aqueous Solution and in the Solid State. *ChemBioChem* **2021**, *22* (5), 826−829.

(9) Métro, T.-X.; Gervais, C.; Martinez, A.; Bonhomme, C.; Laurencin, D. Unleashing the Potential of 17O NMR Spectroscopy Using Mechanochemistry. *Angew. Chem., Int. Ed.* **2017**, *56* (24), 6803−6807.

(10) Pugh, S. M.; Wright, P. A.; Law, D. J.; Thompson, N.; Ashbrook, S. E. Facile, Room-Temperature 17O Enrichment of Zeolite Frameworks Revealed by Solid-State NMR Spectroscopy. *J. Am. Chem. Soc.* **2020**, *142* (2), 900−906.

(11) Špačková, J.; Fabra, C.; Mittelette, S.; Gaillard, E.; Chen, C.-H.; Cazals, G.; Lebrun, A.; Sene, S.; Berthomieu, D.; Chen, K.; Gan, Z.; Gervais, C.; Métro, T.-X.; Laurencin, D. Unveiling the Structure and Reactivity of Fatty-Acid Based (Nano)Materials Thanks to Efficient and Scalable 17O and 18O-Isotopic Labeling Schemes. *J. Am. Chem. Soc.* **2020**, *142* (50), 21068−21081.

(12) Chen, C.; Goldberga, I.; Gaveau, P.; Mittelette, S.; Špačková, J.; Mullen, C.; Petit, I.; Métro, T.; Alonso, B.; Gervais, C.; Laurencin, D. Looking into the Dynamics of Molecular Crystals of Ibuprofen and Terephthalic Acid Using 17O and 2H Nuclear Magnetic Resonance Analyses. *Magn. Reson. Chem.* **2021**, *59* (9−10), 975−990.

(13) Martins, V.; Xu, J.; Wang, X.; Chen, K.; Hung, I.; Gan, Z.; Gervais, C.; Bonhomme, C.; Jiang, S.; Zheng, A.; Lucier, B. E. G.; Huang, Y. Higher Magnetic Fields, Finer MOF Structural Information: O-17 Solid-State NMR at 35.2 T. *J. Am. Chem. Soc.* **2020**, *142* (35), 14877−14889.

(14) Martins, V.; Xu, J.; Hung, I.; Gan, Z.; Gervais, C.; Bonhomme, C.; Huang, Y. 17O Solid-state NMR at Ultrahigh Magnetic Field of 35.2 T: Resolution of Inequivalent Oxygen Sites in Different Phases of MOF MIL-53(Al). *Magn. Reson. Chem.* **2021**, *59* (9−10), 940−950.

(15) Michaelis, V. K.; Markhasin, E.; Daviso, E.; Herzfeld, J.; Griffin, R. G. Dynamic Nuclear Polarization of Oxygen-17. *J. Phys. Chem. Lett.* **2012**, *3* (15), 2030−2034.

(16) Keeler, E. G.; Michaelis, V. K.; Griffin, R. G. 17O NMR Investigation of Water Structure and Dynamics. *J. Phys. Chem. B* **2016**, *120* (32), 7851−7858.

(17) Frydman, L.; Harwood, J. S. Isotropic Spectra of Half-Integer Quadrupolar Spins from Bidimensional Magic-Angle-Spinning NMR. *J. Am. Chem. Soc.* **1995**, *117* (19), 5367−5368.

(18) Gan, Z. Isotropic NMR Spectra of Half-Integer Quadrupolar Nuclei Using Satellite Transitions and Magic-Angle Spinning. *J. Am. Chem. Soc.* **2000**, *122* (13), 3242−3243.

(19) Wu, G. Solid-State 17O NMR Studies of Organic and Biological Molecules. *Prog. Nucl. Magn. Reson. Spectrosc.* **2008**, *52* (2−3), 118−169.

(20) Barbet-Massin, E.; Pell, A. J.; Retel, J. S.; Andreas, L. B.; Jaudzems, K.; Franks, W. T.; Nieuwkoop, A. J.; Hiller, M.; Higman, V.; Guerry, P.; Bertarello, A.; Knight, M. J.; Felletti, M.; Le Marchand, T.; Kotelovica, S.; Akopjana, I.; Tars, K.; Stoppini, M.; Bellotti, V.; Bolognesi, M.; Ricagno, S.; Chou, J. J.; Griffin, R. G.; Oschkinat, H.; Lesage, A.; Emsley, L.; Herrmann, T.; Pintacuda, G. Rapid Proton-Detected NMR Assignment for Proteins with Fast Magic Angle Spinning. *J. Am. Chem. Soc.* **2014**, *136* (35), 12489−12497.

(21) Penzel, S.; Smith, A. A.; Agarwal, V.; Hunkeler, A.; Org, M.-L.; Samoson, A.; Böckmann, A.; Ernst, M.; Meier, B. H. Protein Resonance Assignment at MAS Frequencies Approaching 100 kHz: A Quantitative Comparison of J-Coupling and Dipolar-Coupling-Based Transfer Methods. *J. Biomol. NMR* **2015**, *63* (2), 165−186.

(22) Stanek, J.; Andreas, L. B.; Jaudzems, K.; Cala, D.; Lalli, D.; Bertarello, A.; Schubeis, T.; Akopjana, I.; Kotelovica, S.; Tars, K.; Pica, A.; Leone, S.; Picone, D.; Xu, Z.-Q.; Dixon, N. E.; Martinez, D.; Berbon, M.; El Mammeri, N.; Noubhani, A.; Saupe, S.; Habenstein, B.; Loquet, A.; Pintacuda, G. NMR Spectroscopic Assignment of Backbone and Side-Chain Protons in Fully Protonated Proteins:

Microcrystals, Sedimented Assemblies, and Amyloid Fibrils. *Angew. Chem., Int. Ed.* **2016**, *55* (50), 15504−15509.
(23) Iuga, D.; Morais, C.; Gan, Z.; Neuville, D. R.; Cormier, L.; Massiot, D. NMR Heteronuclear Correlation between Quadrupolar Nuclei in Solids. *J. Am. Chem. Soc.* **2005**, *127* (33), 11540−11541.
(24) Hung, I.; Uldry, A.-C.; Becker-Baldus, J.; Webber, A. L.; Wong, A.; Smith, M. E.; Joyce, S. A.; Yates, J. R.; Pickard, C. J.; Dupree, R.; Brown, S. P. Probing Heteronuclear 15N−17O and 13C−17O Connectivities and Proximities by Solid-State NMR Spectroscopy. *J. Am. Chem. Soc.* **2009**, *131* (5), 1820−1834.
(25) Antzutkin, O. N.; Iuga, D.; Filippov, A. V.; Kelly, R. T.; Becker-Baldus, J.; Brown, S. P.; Dupree, R. Hydrogen Bonding in Alzheimer's Amyloid-β Fibrils Probed by 15N/17O REAPDOR Solid-State NMR Spectroscopy. *Angew. Chem., Int. Ed.* **2012**, *51* (41), 10289−10292.
(26) Carnahan, S. L.; Lampkin, B. J.; Naik, P.; Hanrahan, M. P.; Slowing, I. I.; VanVeller, B.; Wu, G.; Rossini, A. J. Probing O−H Bonding through Proton Detected 1H−17O Double Resonance Solid-State NMR Spectroscopy. *J. Am. Chem. Soc.* **2019**, *141* (1), 441−450.
(27) Hung, I.; Gan, Z.; Wu, G. Two- and Three-Dimensional 13C−17O Heteronuclear Correlation NMR Spectroscopy for Studying Organic and Biological Solids. *J. Phys. Chem. Lett.* **2021**, *12* (36), 8897−8902.
(28) Hung, I.; Gan, Z. Isotropic Solid-State MQMAS NMR Spectra for Large Quadrupolar Interactions Using Satellite-Transition Selective Inversion Pulses and Low Rf Fields. *J. Magn. Reson.* **2021**, *324*, 106913.
(29) Hung, I.; Gan, Z. On the Use of Single-Frequency versus Double-Frequency Satellite-Transition Pulses for MQMAS. *J. Magn. Reson.* **2021**, *328*, 106994.
(30) Akbey, Ü.; Lange, S.; Trent Franks, W.; Linser, R.; Rehbein, K.; Diehl, A.; van Rossum, B.-J.; Reif, B.; Oschkinat, H. Optimum Levels of Exchangeable Protons in Perdeuterated Proteins for Proton Detection in MAS Solid-State NMR Spectroscopy. *J. Biomol. NMR* **2010**, *46* (1), 67−73.
(31) Vega, A. J. MAS NMR Spin Locking of Half-Integer Quadrupolar Nuclei. *J. Magn. Reson.* **1992**, *96* (1), 50−68.
(32) Vega, A. J. CP/MAS of Quadrupolar S = 3/2 Nuclei. *Solid State Nucl. Magn. Reson.* **1992**, *1* (1), 17−32.
(33) Ashbrook, S. E.; Wimperis, S. Spin-Locking of Half-Integer Quadrupolar Nuclei in Nuclear Magnetic Resonance of Solids: Creation and Evolution of Coherences. *J. Chem. Phys.* **2004**, *120* (6), 2719−2731.
(34) Ashbrook, S. E.; Wimperis, S. Spin-Locking of Half-Integer Quadrupolar Nuclei in Nuclear Magnetic Resonance of Solids: Second-Order Quadrupolar and Resonance Offset Effects. *J. Chem. Phys.* **2009**, *131* (19), 194509.
(35) Lim, K. H.; Grey, C. P. 19F/23Na Cross Polarization NMR Study of Hydrofluorocarbon−Zeolite Binding on Zeolite NaY. *Chem. Commun.* **1998**, No. 20, 2257−2258.
(36) Egan, J. M.; Mueller, K. T. Detection and Identification of Corrosion Products of Sodium Aluminoborosilicate Glasses by 23Na MQMAS and 1H → 23Na CPMAS NMR. *J. Phys. Chem. B* **2000**, *104* (41), 9580−9586.
(37) Peng, L.; Huo, H.; Liu, Y.; Grey, C. P. 17O Magic Angle Spinning NMR Studies of Brønsted Acid Sites in Zeolites HY and HZSM-5. *J. Am. Chem. Soc.* **2007**, *129* (2), 335−346.
(38) Brownbill, N. J.; Gajan, D.; Lesage, A.; Emsley, L.; Blanc, F. Oxygen-17 Dynamic Nuclear Polarisation Enhanced Solid-State NMR Spectroscopy at 18.8 T. *Chem. Commun.* **2017**, *53* (17), 2563−2566.
(39) Carnevale, D.; Mouchaham, G.; Wang, S.; Baudin, M.; Serre, C.; Bodenhausen, G.; Abergel, D. Natural Abundance Oxygen-17 Solid-State NMR of Metal Organic Frameworks Enhanced by Dynamic Nuclear Polarization. *Phys. Chem. Chem. Phys.* **2021**, *23* (3), 2245−2251.
(40) Meier, B. H. Cross Polarization under Fast Magic Angle Spinning - Thermodynamical Considerations. *Chem. Phys. Lett.* **1992**, *188* (3−4), 201−207.
(41) Gan, Z. Spin Dynamics of Polarization Inversion Spin Exchange at the Magic Angle in Multiple Spin Systems. *J. Magn. Reson.* **2000**, *143* (1), 136−143.
(42) Bayro, M. J.; Huber, M.; Ramachandran, R.; Davenport, T. C.; Meier, B. H.; Ernst, M.; Griffin, R. G. Dipolar Truncation in Magic-Angle Spinning NMR Recoupling Experiments. *J. Chem. Phys.* **2009**, *130* (11), 114506.
(43) Nagashima, H.; Trébosc, J.; Kon, Y.; Sato, K.; Lafon, O.; Amoureux, J.-P. Observation of Low-γ Quadrupolar Nuclei by Surface-Enhanced NMR Spectroscopy. *J. Am. Chem. Soc.* **2020**, *142* (24), 10659−10672.
(44) Gan, Z. H.; Amoureux, J. P.; Trebosc, J. Proton-Detected N-14 MAS NMR Using Homonuclear Decoupled Rotary Resonance. *Chem. Phys. Lett.* **2007**, *435* (1−3), 163−169.
(45) Cavadini, S.; Abraham, A.; Bodenhausen, G. Proton-Detected Nitrogen-14 NMR by Recoupling of Heteronuclear Dipolar Interactions Using Symmetry-Based Sequences. *Chem. Phys. Lett.* **2007**, *445* (1−3), 1−5.
(46) Venkatesh, A.; Luan, X.; Perras, F. A.; Hung, I.; Huang, W.; Rossini, A. J. T(1)-Noise Eliminated Dipolar Heteronuclear Multiple-Quantum Coherence Solid-State NMR Spectroscopy. *Phys. Chem. Chem. Phys.* **2020**, *22* (36), 20815−20828.
(47) Laage, S.; Marchetti, A.; Sein, J.; Pierattelli, R.; Sass, H. J.; Grzesiek, S.; Lesage, A.; Pintacuda, G.; Emsley, L. Band-Selective H-1-C-13 Cross-Polarization in Fast Magic Angle Spinning Solid-State NMR Spectroscopy. *J. Am. Chem. Soc.* **2008**, *130* (51), 17216−17217.
(48) Lange, A.; Scholz, I.; Manolikas, T.; Ernst, M.; Meier, B. H. Low-Power Cross Polarization in Fast Magic-Angle Spinning NMR Experiments. *Chem. Phys. Lett.* **2009**, *468* (1−3), 100−105.
(49) Demers, J. P.; Vijayan, V.; Becker, S.; Lange, A. Tailored Low-Power Cross-Polarization under Fast Magic-Angle Spinning. *J. Magn. Reson.* **2010**, *205* (2), 216−223.
(50) Wokaun, A.; Ernst, R. R. Selective Excitation and Detection in Multilevel Spin Systems: Application of Single Transition Operators. *J. Chem. Phys.* **1977**, *67* (4), 1752−1758.
(51) Oas, T. G.; Griffin, R. G.; Levitt, M. H. Rotary Resonance Recoupling of Dipolar Interactions in Solid-State Nuclear Magnetic-Resonance Spectroscopy. *J. Chem. Phys.* **1988**, *89* (2), 692−695.
(52) Nielsen, N. C.; Bildsoe, H.; Jakobsen, H. J.; Levitt, M. H. Double-Quantum Homonuclear Rotary Resonance - Efficient Dipolar Recovery in Magic-Angle-Spinning Nuclear-Magnetic-Resonance. *J. Chem. Phys.* **1994**, *101* (3), 1805−1812.
(53) Ye, Y. Q.; Malon, M.; Martineau, C.; Taulelle, F.; Nishiyama, Y. Rapid Measurement of Multidimensional 1H Solid-State NMR Spectra at Ultra-Fast MAS Frequencies. *J. Magn. Reson.* **2014**, *239*, 75−80.
(54) Chevelkov, V.; van Rossum, B. J.; Castellani, F.; Rehbein, K.; Diehl, A.; Hohwy, M.; Steuernagel, S.; Engelke, F.; Oschkinat, H.; Reif, B. 1H Detection in MAS Solid-State NMR Spectroscopy of Biomacromolecules Employing Pulsed Field Gradients for Residual Solvent Suppression. *J. Am. Chem. Soc.* **2003**, *125* (26), 7788−7789.
(55) Agarwal, V.; Diehl, A.; Skrynnikov, N.; Reif, B. High Resolution 1H Detected 1H, 13C Correlation Spectra in MAS Solid-State NMR Using Deuterated Proteins with Selective 1H, 2H Isotopic Labeling of Methyl Groups. *J. Am. Chem. Soc.* **2006**, *128* (39), 12620−12621.
(56) Hayashi, S.; Hayamizu, K. Line-Shapes in CP/MAS NMR-Spectra of Half-Integer Quadrupolar Nuclei. *Chem. Phys. Lett.* **1993**, *203* (4), 319−324.
(57) Barrie, P. J. Distorted Powder Lineshapes in 27Al CP/MAS NMR Spectroscopy of Solids. *Chem. Phys. Lett.* **1993**, *208* (5−6), 486−490.
(58) Hayashi, S. Magic-Angle Spinning Nuclear Magnetic Resonance of Half-Integer Quadrupole Nuclei: Effect of Spin-Locking Efficiency on Powder Lineshapes. *Solid State Nucl. Magn. Reson.* **1994**, *3* (2), 93−101.
(59) Ding, S. W.; Mcdowell, C. A. Theoretical Calculations of the CPMAS Spectral Lineshapes of Half-Integer Quadrupole Systems. *J. Magn. Reson. A* **1995**, *114* (1), 80−87.

https://doi.org/10.1021/acs.jpclett.2c01777
J. Phys. Chem. Lett. 2022, 13, 6549−6558

(60) Linser, R.; Fink, U.; Reif, B. Narrow Carbonyl Resonances in Proton-Diluted Proteins Facilitate NMR Assignments in the Solid-State. *J. Biomol. NMR* **2010**, *47* (1), 1−6.
(61) Verel, R.; Baldus, M.; Ernst, M.; Meier, B. H. A Homonuclear Spin-Pair Filter for Solid-State NMR Based on Adiabatic-Passage Techniques. *Chem. Phys. Lett.* **1998**, *287* (3−4), 421−428.
(62) Kay, L. E.; Ikura, M.; Tschudin, R.; Bax, A. Three-Dimensional Triple-Resonance NMR Spectroscopy of Isotopically Enriched Proteins. *J. Magn. Reson.* **1990**, *89* (3), 496−514.
(63) Grzesiek, S.; Bax, A. Improved 3D Triple-Resonance NMR Techniques Applied to a 31 KDa Protein. *J. Magn. Reson.* **1992**, *96* (2), 432−440.
(64) Becerra, L. R.; Gerfen, G. J.; Temkin, R. J.; Singel, D. J.; Griffin, R. G. Dynamic Nuclear Polarization with a Cyclotron Resonance Maser at 5 T. *Phys. Rev. Lett.* **1993**, *71* (21), 3561−3564.
(65) Maly, T.; Debelouchina, G. T.; Bajaj, V. S.; Hu, K.-N.; Joo, C.-G.; Mak−Jurkauskas, M. L.; Sirigiri, J. R.; van der Wel, P. C. A.; Herzfeld, J.; Temkin, R. J.; Griffin, R. G. Dynamic Nuclear Polarization at High Magnetic Fields. *J. Chem. Phys.* **2008**, *128* (5), 052211.
(66) Can, T. V.; Ni, Q. Z.; Griffin, R. G. Mechanisms of Dynamic Nuclear Polarization in Insulating Solids. *J. Magn. Reson.* **2015**, *253*, 23−35.
(67) Brinkmann, A.; Kentgens, A. P. M. Proton-Selective O-17-H-1 Distance Measurements in Fast Magic-Angle-Spinning Solid-State NMR Spectroscopy for the Determination of Hydrogen Bond Lengths. *J. Am. Chem. Soc.* **2006**, *128* (46), 14758−14759.
(68) Kupce, E.; Freeman, R. Adiabatic Pulses for Wide-Band Inversion and Broad-Band Decoupling. *J. Magn. Reson. A* **1995**, *115* (2), 273−276.
(69) Trease, N. M.; Dey, K. K.; Grandinetti, P. J. Optimum Excitation of "Enhanced" Central Transition Populations. *J. Magn. Reson.* **2009**, *200* (2), 334−339.
(70) Massiot, D.; Touzo, B.; Trumeau, D.; Coutures, J. P.; Virlet, J.; Florian, P.; Grandinetti, P. J. Two-Dimensional Magic-Angle Spinning Isotropic Reconstruction Sequences for Quadrupolar Nuclei. *Solid State Nucl. Magn. Reson.* **1996**, *6* (1), 73−83.
(71) Brown, S. P.; Wimperis, S. Two-Dimensional Multiple-Quantum MAS NMR of Quadrupolar Nuclei: A Comparison of Methods. *J. Magn. Reson.* **1997**, *128* (1), 42−61.
(72) Venkatesh, A.; Hanrahan, M. P.; Rossini, A. J. Proton Detection of MAS Solid-State NMR Spectra of Half-Integer Quadrupolar Nuclei. *Solid State Nucl. Magn. Reson.* **2017**, *84*, 171−181.
(73) Harris, R. K.; Becker, E. D.; De Menezes, S. M. C.; Goodfellow, R.; Granger, P. NMR Nomenclature. Nuclear Spin Properties and Conventions for Chemical Shifts - (IUPAC Recommendations 2001). *Pure Appl. Chem.* **2001**, *73* (11), 1795−1818.
(74) Amoureux, J. P.; Huguenard, C.; Engelke, F.; Taulelle, F. Unified Representation of MQMAS and STMAS NMR of Half-Integer Quadrupolar Nuclei. *Chem. Phys. Lett.* **2002**, *356* (5−6), 497−504.

https://doi.org/10.1021/acs.jpclett.2c01777
J. Phys. Chem. Lett. 2022, 13, 6549−6558